sustainability

MDPI

Article

Remote Sensing Evidence for Significant Variations in the Global Gross Domestic Product during the COVID-19 Epidemic

Bin Guo [1,*,†], Wencai Zhang [1,†], Lin Pei [2,*], Xiaowei Zhu [3], Pingping Luo [4] and Weili Duan [5]

1 College of Geomatics, Xi'an University of Science and Technology, Xi'an 710054, China
2 School of Exercise and Health Sciences, Xi'an Physical Education University, Xi'an 710068, China
3 Department of Mechanical and Materials Engineering, Portland State University, Portland, OR 97207, USA
4 School of Water and Environment, Chang'an University, Xi'an 710054, China
5 State Key Laboratory of Desert and Oasis Ecology, Xinjiang Institute of Ecology and Geography, Chinese Academy of Sciences, Urumqi 830011, China
* Correspondence: guobin12@xust.edu.cn (B.G.); pl880512@stu.xjtu.edu.cn (L.P.)
† These authors contributed equally to this work.

Abstract: Coronavirus disease 2019 (COVID-19) has been spreading rapidly and is still threatening human health currently. A series of measures for restraining epidemic spreading has been adopted throughout the world, which seriously impacted the gross domestic product (GDP) globally. However, details of the changes in the GDP and its spatial heterogeneity characteristics on a fine scale worldwide during the pandemic are still uncertain. We designed a novel scheme to simulate a $0.1° \times 0.1°$ resolution grid global GDP map during the COVID-19 pandemic. Simulated nighttime-light remotely sensed data (SNTL) was forecasted via a GM(1, 1) model under the assumption that there was no COVID-19 epidemic in 2020. We constructed a geographically weighted regression (GWR) model to determine the quantitative relationship between the variation of nighttime light (ΔNTL) and the variation of GDP (ΔGDP). The scheme can detect and explain the spatial heterogeneity of ΔGDP at the grid scale. It is found that a series of policies played an obvious role in affecting GDP. This work demonstrated that the global GDP, except for in a few countries, represented a remarkably decreasing trend, whereas the ΔGDP exhibited significant differences.

Keywords: GDP prediction; GM(1, 1); GWR; NPP-VIIRS; COVID-19

check for updates

Citation: Guo, B.; Zhang, W.; Pei, L.; Zhu, X.; Luo, P.; Duan, W. Remote Sensing Evidence for Significant Variations in the Global Gross Domestic Product during the COVID-19 Epidemic. *Sustainability* **2022**, *14*, 15201. https://doi.org/10.3390/su142215201

Academic Editor: Chao Tao

Received: 6 September 2022
Accepted: 12 November 2022
Published: 16 November 2022

1. Introduction

Since Coronavirus Disease 2019 (COVID-19) first broke out, it has infected more than 435 million people [1] and caused millions of deaths globally [2]. As the disease has severely threatened public health, serious restrictions for preventing the spread of COVID-19 have been adopted worldwide [3], which provides a rare opportunity for exploring how a global public health emergency could impact the environment and economy [4].

It is confirmed that the pandemic has posed significant impacts on anthropic emissions and atmospheric environment quality [5,6], ecology [7,8], and the global economy [9]. Firstly, reduced anthropogenic emissions and decreased aerosol optical depth (AOD) was proven due to restrictions on anthropic activities during the COVID-19 epidemic [5,7]. Meanwhile, population-weighted mean $PM_{2.5}$ (particulate matter smaller than 2.5 μm) concentrations were proven to decrease by 11 to 15 μg/m^3 during the lockdown in China, Europe, and North America in 2020 compared with the corresponding time in 2018 to 2019 largely owing to a series of transportation restriction measures [10]. Secondly, decreasing human activities during the pandemic generated obvious effects on the ecological environment worldwide. Specifically, COVID-19 restrictions led to an earlier, greener, and brighter spring season in China in 2020, which further suggested that reductions in human activities generated significant effects on the ecological environment [7]. Although economic development was seriously influenced due to restrictions on human activities, biodiversity received benefits to some extent [11]. For example, marine animals started to roam more frequently than ever before owing to reductions in marine traffic and noise deduction. Some unusual animals were found in urban environments because of the decreased interference of humans.

Thirdly, the global economy was remarkably affected due to the COVID-19 epidemic. Previous studies estimated the pandemic posed negative effects on economic development. The impact of the epidemic on the gross domestic product (GDP) was much stronger than that of the financial crisis in 2008; the world economic growth rate has slowed from an average of 4.63% (2000–2007) to an average of 3.4% (2008–2018). The International Monetary Fund (IMF) reported that global economic growth has dropped from 2.8% in 2019 to −3.3% in 2020 due to the COVID-19 pandemic [12]. Countries all over the world have implemented control measures such as lockdowns that strongly restrict human activities, which account for the slowing in economic development globally [5]. The GDP of Europe in 2020 decreased by −5.8% compared with the previous year 2019, following North America by −4.1%, and Asia and the Pacific by −1.3%, respectively [8]. Additionally, one published paper indicated that lockdowns of longer duration posed negative effects on GDP growth. This finding demonstrated a systematic deterioration of the economic system owing to containment policies based on a longer duration of lockdown in society [13]. Moreover, mobility declined significantly both for long-distance air travel and for surface transportation [8]. In addition, about 90–150 million people could fall into extreme poverty because of the pandemic [14]. Food shortage and poverty phenomena have occurred because of the decrease in agricultural products, the shortages of labor, and deductions of incomes, which may increase the risks of food security and inadequate nutrition [9].

GDP is a significant metric to assess the economic situation and development status of a country or region [13]. As an important aspect, the impacts of COVID-19 on the GDP at the regional scale have been explored. However, the precision was inadequate to indicate the spatial heterogeneity of the GDP variations on a global scale [15], and assessing this at the grid scale due to the pandemic is still a big challenge [16]. The traditional GDP estimation methods are, on the one hand, severely restricted by spatiotemporal resolution, effectiveness, and finance consumption, and on the other hand, easily affected by human opinion, which thus has difficult to use on a global scale. For example, plenty of algorithms have been implemented to evaluate more precise GDP previously, including the cash-demand method [17], the consumer expenditure method [18], and the multiple indicators/multiple cause (MIMIC) algorithm [17]. The Difference-in-Differences technique was widely used to detect the policy effects on GDP, but it can hardly be utilized to infer GDP variations at a grid scale [19]. Fortunately, the geographically weighted regression (GWR) model has been proven to be effective in solving local modeling and estimating social-economic parameters at the grid scale [20].

Recently, remotely sensed technology has been widely used to monitor human activities and the physical environment dynamic [21]. Specifically, remotely sensed technology largely supports scientists in studying environmental and socioeconomic issues at global or regional scales with swift responses [22]. For example, the ability of nighttime light (NTL) images in estimating socioeconomic parameters has been proven, which supplies a novel perspective for reflecting human activities. NTL images are adaptable for inferring GDP, population [23], electricity consumption, greenhouse gas emissions, poverty, and urbanization [24]. Additionally, NTL images have been successfully used to address some unusual issues, such as war [25], natural disasters [26], large-scale power outages [27], fishing activities [28], light pollution [29], and human physiological and psychological health [30], etc. Currently, the NTL data have also been introduced to detect human mobility and economic activities during the period of COVID-19 in 2020 [31,32]. For instance, the change trends of NTL probably generated by changes in human activities due to restrictions during pandemics have been captured by nighttime-light remotely sensed technology. The change detection for the NTL value was conducted via comparisons between epidemic periods and corresponding periods of the previous year. The NTL indicated lights in China, Morocco, and India were dimming during the COVID-19 pandemic period accounting for the lockdown measures adopted by the governments [31,32]. Obviously, previous studies confirmed that the artificial light changing trend can be effectively detected using nighttime-light remotely sensed satellites [33]. NTL can be selected as a trustworthy proxy to monitor the decline and recovery in economic activities and to further understand the impact of the COVID-19 epidemic on human activities and the economy [34]. The variation in NTL was indirectly used to reflect variation in GDP during the COVID-19 pandemic previously [31,34]. For example, the comparison of NTL images from before and after the outbreak of COVID-19 has been conducted, and the variation in NTL was used to qualitatively approximatively describe the variation in GDP during the COVID-19 pandemic [33,34]. However, previous studies ignored the natural economic growth of human societies that would have occurred if there had been no COVID-19 pandemic in 2020, and the quantitative estimation of GDP variation globally during the COVID-19 pandemic has never been considered to date.

To address the above issues, the present study aims (1) to obtain simulated NTL (SNTL) images via a GM(1, 1) model under the assumption that there was no COVID-19 epidemic in 2020, (2) to calculate the deviation (ΔNTL) between observed actual NTL (ANTL) and the SNTL using ArcGIS10.0, and (3) to determine the quantitative relationship between ΔNTL and the variation of GDP(ΔGDP) via the geographically weighted regression (GWR) model and map the ΔGDP at a $0.1^\circ \times 0.1^\circ$ scale globally in 2020.

2. Materials and Methods

2.1. Study Areas

One hundred and fifty-one major countries globally were selected as study areas in the current work (Figure 1). Other countries were excluded because statistics or COVID-19 infection data were not available or not consistent. Countries with ambiguous COVID-19 statistics and small GDP totals were excluded from consideration in this study. After data screening, 151 countries were finally retained as the study area.

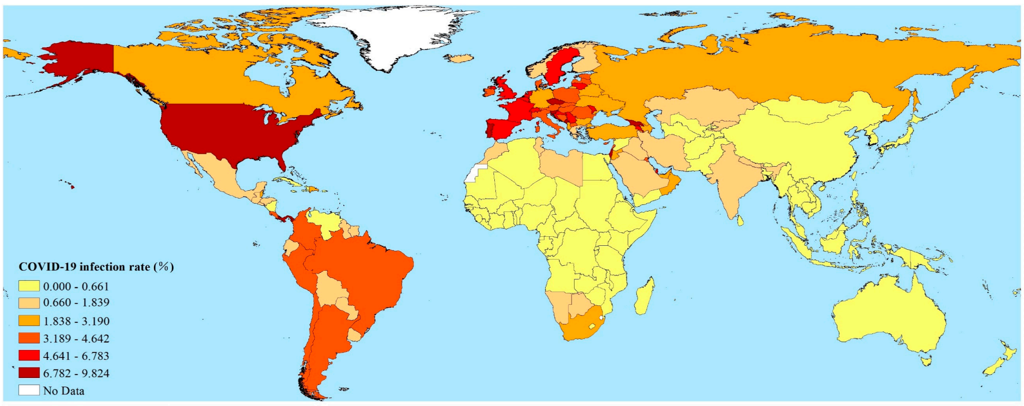

Figure 1. The map of the COVID-19 infection rate by January 2021 globally. Note: the COVID-19 infection rate was calculated by dividing the total COVID-19 infection cases by the total population.

2.2. Data Source and Preprocessing

National demographics population data from 2020 were merged from the IMF and the United Nations Department of Economic and Social Affairs (UN DESA). Similarly, population data were also pretreated by screening and comparison for keeping the correctness for each country in 2020.

The country boundary file, with the WGS-84 coordinate system, was obtained from the Institute of Geographic Sciences and Natural Resources Research, Chinese Academy of Sciences (Table 1). One hundred and fifty-one country boundaries were consistent with the above datasets.

Table 1. Data sources and descriptions.

Data Sorts	Data Description	Study Duration
NPP/VIIRS NTL imagery	NPP/VIIRS monthly images	2013–2020
Population	The population is presented in thousands	2020
COVID-19 epidemic-related data	Cumulative cases and deaths of each country	2020
GDP, current prices	Billions of U.S. dollars	2013–2020
Country boundary file	Shape format	2015

2.3. Methods

To quickly and accurately assess GDP changes in the face of the COVID-19 pandemic, nightlight remote sensing images were selected as a proxy to infer GDP globally. The workflow of this study was shown as follows (Figure 2). Firstly, we conducted data preparation for further model fitting and mapping. Secondly, SNTL was predicted via a GM(1, 1) model using global NTL images from 2013 to 2019 under the assumption that there was no COVID-19 pandemic in 2020. Thirdly, the ΔNTL image was determined by the ANTL image, deducting the SNTL image from 2020. Then, the total ΔNTL values of NTL remotely sensed data at the country scale were summarized using the zonal statistics tool ArcGIS 10.0. Similarly, the ΔGDP data at the country scale were calculated by the actual GDP (GDP_a) data obtained from the IMF, deducting the predicted GDP (GDP_f) data forecasted by the IMF for 2020. Furthermore, GWR was introduced for calibrating ΔGDP at the national scale. The performance of the GWR model was evaluated by cross-validation on the national scale. Finally, the GWR model was downscaled for mapping the ΔGDP at the grid scale globally, and the spatial distribution features of the ΔGDP were indicated.

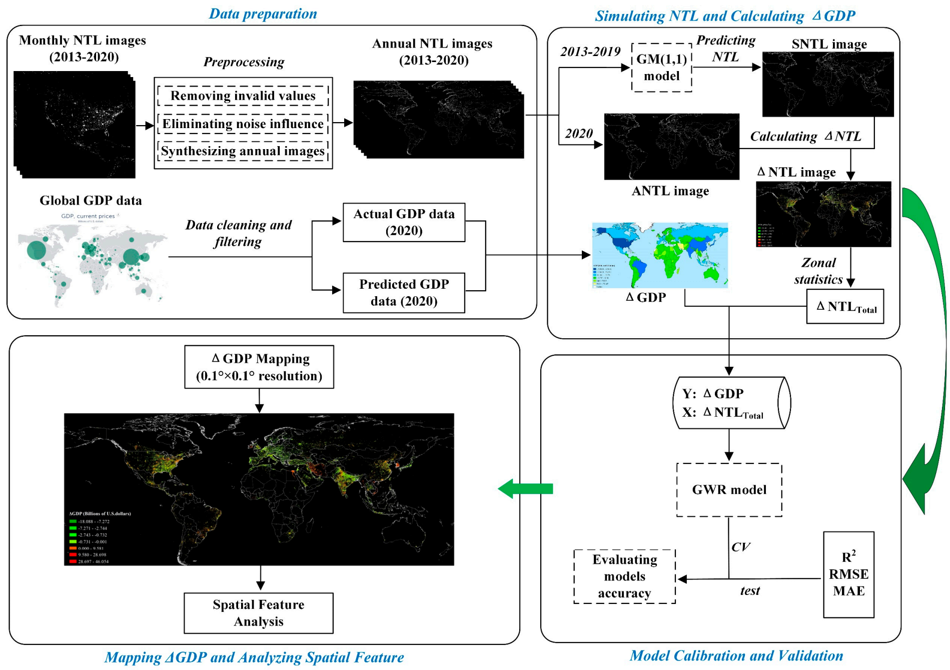

Figure 2. The workflow of this study.

2.3.1. Simulating the NTL Image

Professor Julong Deng proposed the Grey System Theory (GST) in the 1980s, and GM(1, 1) is one of the most important models of the GST [35]. The GM(1, 1) model for solving grey forecasting issues, with a compatible model group including differential, difference, and exponential models, has been widely used in addressing uncertain issues [36]. Published papers have proved that the GM(1, 1) model can be used in dealing with grey forecasting issues, and the reliability of the GM(1, 1) model is accepted in addressing uncertain problems [35,37].

The NTL was significantly affected by the COVID-19 pandemic which was a classic uncertain issue and can be simulated by the GM(1, 1) model. Therefore, the GM(1, 1) model was introduced to simulate NTL under the assumption of no epidemic spreading in 2020. Before simulating the NTL image of 2020, the performance of the GM(1, 1) model in simulating the NTL image in 2019 based on the NTL image from 2013 to 2018 was validated by the actual NTL image from 2019 via the coefficient of determination (R^2), the root mean square error (RMSE), and the Mean Absolute Error (MAE). Cross-validation was conducted as follows. Firstly, we used NTL images from the years 2013–2018 to fit the GM(1, 1) model for predicting NTL images of the year 2019 (SNTL). Secondly, cross-validation was conducted between the SNTL of the year 2019 and actual NTL images from the year 2019 on both national scales and grid scales. Finally, the SNTL image for 2020 under the assumption of no COVID-19 pandemic was obtained by GM(1, 1). The steps of the GM(1, 1) model are shown as follows:

(1) Set all NTL images from 2013 to 2019 as the original sequence with respect to time:

$$X^{(0)} = (x_1^{(0)}, x_2^{(0)}, \ldots, x_n^{(0)}) \tag{1}$$

where $X^{(0)}$ represents the original sequence and $x_i^{(0)}$ represents the NTL image in a specific year i; i is from 1 to 8 in the current study.

(2) 1-AGO (Accumulated Generating Operation) was performed to the original sequence $X^{(0)}$ for a regular sequence $X^{(1)}$ below:

$$X^{(1)} = (x_1^{(1)}, x_2^{(1)}, \ldots, x_n^{(1)}) \tag{2}$$

where $x_k^{(1)}$ was determined as follows:

$$x_k^{(1)} = \sum\nolimits_{i=1}^{k} x_i^{(0)}, k = i, 2, \ldots, n \tag{3}$$

where $x_k^{(1)}$ denotes the elements in the regular sequence; k is from 1 to 8 in the current study.

(3) The sequence of mean generation of consecutive neighbors $Z^{(1)}$ was calculated from $X^{(1)}$:

$$Z^{(1)} = (z_2^{(1)}, z_3^{(1)}, \ldots, z_n^{(1)}) \tag{4}$$

$$z_k^{(1)} = 0.5x_{k-1}^{(1)} + 0.5x_k^{(1)}, k = 2, 3 \ldots, n \tag{5}$$

where $Z^{(1)}$ denotes the sequence of consecutive neighbors of the AGO sequence $X^{(1)}$. $z_k^{(1)}$ denotes the elements in the sequence of consecutive neighbors.

(4) So, GM(1, 1) is defined below:

$$x_k^{(0)} + az_k^{(1)} = b \tag{6}$$

where the definition of $x_k^{(0)}$ and $z_k^{(1)}$ are the same as (1) and (5), and a and b are the development coefficient and the ash effect, respectively. a and b in Equation (6) were determined via a least square estimate as follows.

If $\hat{a} = (a, b)^T$ is the parameter of the GM(1, 1) model, and:

$$B = \begin{bmatrix} -\frac{1}{2}(x_1^{(1)} + x_2^{(1)}) & 1 \\ -\frac{1}{2}(x_2^{(1)} + x_3^{(1)}) & 1 \\ \vdots & \vdots \\ -\frac{1}{2}(x_{n-1}^{(1)} + x_n^{(1)}) & 1 \end{bmatrix}, Y = \begin{bmatrix} x_2^{(0)} \\ x_3^{(0)} \\ \vdots \\ x_n^{(0)} \end{bmatrix} \tag{7}$$

$$Y = B\hat{a} \tag{8}$$

where B and Y denote the independent variable matrix and dependent variable matrix of formula (8), respectively, $\hat{a}$ denotes the column vector of $[a, b]$.

$$\hat{a} = (a, b)^T = \left(B^T \times B\right)^{-1} B^T Y \tag{9}$$

(5) The following equation:

$$\frac{dx^{(1)}}{dt} + ax^{(1)} = b \tag{10}$$

where Equation (10) is named as the whitenization function, $\frac{dx^{(1)}}{dt}$ is the derivative of a continuous function.

(6) The solution of Equation (10):

$$x_t^{(1)} = \left(x_1^{(1)} - \frac{b}{a}\right)e^{-at} + \frac{b}{a} \tag{11}$$

where Equation (11) is named as a time-response function, and t and e denote the continuous variable and the Euler number, respectively.

(7) The corresponding sequence:

$$\hat{x}_{k+1}^{(1)} = \left(x_1^{(0)} - \frac{b}{a}\right)e^{-ak} + \frac{b}{a}, k = 1, 2, \ldots, n \tag{12}$$

where Equation (12) is named as the time-response sequence, and $\hat{x}_{k+1}^{(1)}$ denotes the elements in the corresponding sequence.

Then, the simulated NTL image from Equation (11) was calculated below:

$$\hat{x}_{k+1}^{(0)} = \hat{x}_{k+1}^{(1)} - \hat{x}_k^{(1)} \tag{13}$$

where $\hat{x}_{k+1}^{(0)}$ represents the SNTL in 2020.

2.3.2. Calculating ΔGDP and ΔNTL

ΔGDP was selected to describe the variation of GDP due to the COVID-19 pandemic. One hypothesis must be indicated that the change of GDP in 2020 was mainly caused by the pandemic, and other possible impact factors were neglected in the present study (Equation (14)).

$$\Delta\mathrm{GDP} = \mathrm{GDP_a} - \mathrm{GDP_f} \tag{14}$$

where ΔGDP represents the variation of GDP at the national scale in 2020. Both $\mathrm{GDP_a}$ and $\mathrm{GDP_f}$ were obtained from the IMF, and represent the observed actual GDP and forecasted GDP in 2020, respectively.

ΔNTL was chosen to reflect the dynamic of anthropic activities owing to COVID-19 in 2020 (Equation (15)).

$$\Delta\mathrm{NTL} = \mathrm{ANTL} - \mathrm{SNTL} \tag{15}$$

where ΔNTL represents the deduction between the ANTL and the SNTL in 2020.

2.3.3. Calculating $\Delta\mathrm{NTL_{Total}}$

The $\Delta\mathrm{NTL_{Total}}$ describes the total radiance brightness of ΔNTL. The $\Delta\mathrm{NTL_{Total}}$ denotes the total ΔNTL value that was measured by the zonal statistic of ArcGIS 10.0 in each country. $\Delta\mathrm{NTL_{Total}}$ is also selected as the independent variable for GWR modeling in Section 2.3.4. [38,39].

$$\Delta\mathrm{NTL}_{Total} = \sum_{i=T}^{DN_{max}} (n_i \times DN_i) \tag{16}$$

where DN_i and n_i represent each cell value and the number of cells with the i cell value in a political division, respectively. DN_{max} and T are the maximum and minimum cell values in a political division, respectively.

2.3.4. Fitting GWR Model

The GWR model improves on the ordinary least squares (OLS) regression model by incorporating spatial variation into the coefficient estimation of the explanatory variables in regression models. This study used the GWR model to construct the quantitative relationship between ΔNTL and ΔGDP, which enables us to reveal the spatial heterogeneity of the relationship between ΔNTL and ΔGDP. The GWR model was fitted using ΔGDP in Equation (14) and ΔNTL data in Equation (15) (Equation (17)) [20].

$$\Delta\mathrm{GDP_i} = \beta_{1(u_i,v_i)} + \beta_{2(u_i,v_i)}\cdot\Delta\mathrm{NTL_{Total}} + \varepsilon_i \quad (17)$$

where $\Delta\mathrm{GDP_i}$ is the value of ΔGDP simulated by the GWR model in county i, the definition of $\Delta\mathrm{NTL_{Total}}$ being the same as in Equation (16); β_1 denotes the intercepts at a specific location (u_i, v_i); and β_2 is the location-specific slope. The location (u_i, v_i) represents the central coordinates of a specific country; ε_i is the bias term for county i (i from 1 to 151). Several statistical indicators including R^2, RMSE, and MAE were used to assess model precision. The expression of the above indicators was not stated due to limited space.

2.3.5. Spatial Distribution Characteristics of ΔGDP′

Equations (18) and (19) were used to correct the ΔGDP′ downscaled by Equation (17) on a 0.1° × 0.1° grid scale globally [38,39].

$$\Delta\mathrm{GDP}\prime = \Delta\mathrm{GDP_j} \times \frac{\Delta\mathrm{GDP}}{\Delta\mathrm{GDP_i}} \quad (18)$$

where ΔGDP′ denotes the value of $\Delta\mathrm{GDP_j}$ after correction on the j grid and i political region; $\Delta\mathrm{GDP_j}$ denotes the value of ΔGDP simulated by GWR on the j grid; the definitions of ΔGDP and $\Delta\mathrm{GDP_i}$ are the same as in Equations (14) and (17), respectively.

Although Equation (18) can significantly correct the bias of ΔGDP′ on a grid scale, the relationship between ΔGDP and ΔNTL was ignored. Thus, this study introduces a normalization coefficient as a weight to adjust the ΔGDP′. The final ΔGDP′ map was determined by ΔGDP′ multiplying X_{norm}.

$$X_{norm} = \frac{X_i - X_{min}}{X_{max} - X_{min}} \quad (19)$$

where X_i represents DN value of ΔNTL on the i grid; X_{max} and X_{min} represent the maximum and the minimum DN values of the ΔNTL, respectively. X_{norm} represents the normalization coefficient of ΔNTL ($X_{norm} \in [0, 1]$).

3. Results

3.1. Evaluating GM(1, 1) Model Performance

The performance of the GM(1, 1) model in predicting the NTL image for 2019 was evaluated by cross-validation using three criteria, namely the R^2, the RMSE, and the MAE on national scales and grid scales (Figure 3). It is observed that the model has a better performance at national scales (R^2 = 0.9979, RMSE = 336.4794, MAE = 139.7872) than at grid scales (R^2 = 0.7598, RMSE = 0.8311, MAE = 0.0380).

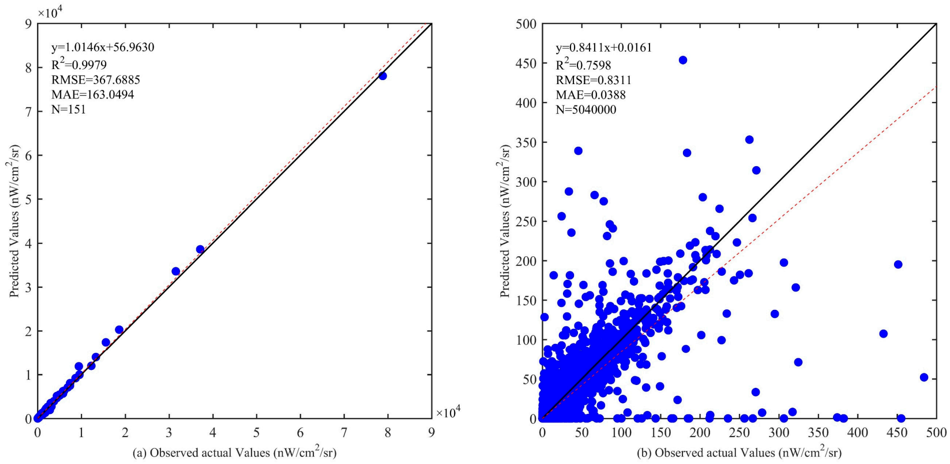

Figure 3. Scatter plots of the GM(1, 1) model performance evaluation. (**a**) and (**b**) show the performance of GM(1, 1) in estimating NTL in 2019 on national scales and grid scales, respectively.

3.2. Calculating ΔNTL Image by ANTL and SNTL

The NTL in the majority of regions decreased globally. The ANTL brightness in 2020 decreased by 8.28% compared with the SNTL in 2020 simulated under the assumption of there being no COVID-19 pandemic. The NTL of major economies across six continents was significantly affected by the COVID-19 pandemic except for Antarctica and other minority regions (Figure 4A).

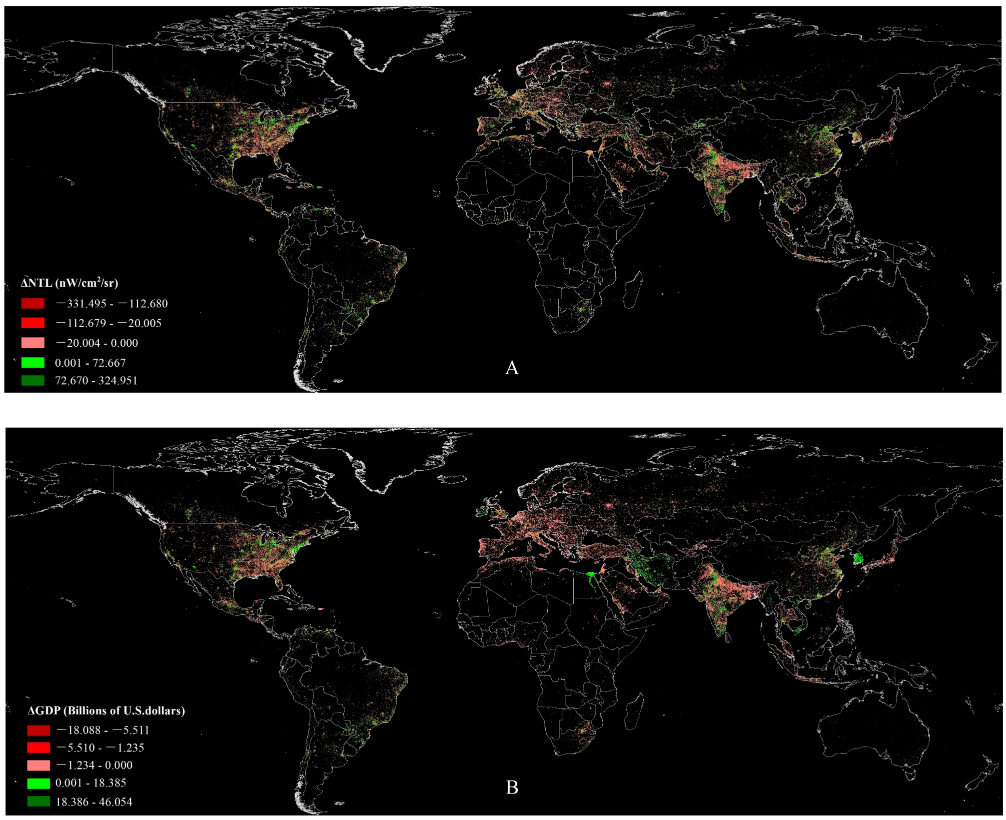

Figure 4. The map of ΔNTL and ΔGDP. The $0.1° \times 0.1°$ resolution map of ΔNTL (**A**) and ΔGDP (**B**) for 151 countries around the world in 2020.

For China, the overall brightness of NTL decreased by 5.19%, and the regions with brightness increasing account for 44.56%, whereas those with decreasing brightness account for 55.44% (Table 2). The remarkable differences in the ΔNTL were divided by the Hu line [40]. The NTL variations were mainly distributed east of the Hu line, whereas the NTL changes west of the Hu line were relatively subtle, especially in Tibet and Qinghai.

Table 2. Statistics for ΔNTL affected by the COVID-19 pandemic.

Location	Total NTL Grids	Grids and Proportion of the NTL Increased	Grids and Proportion of the NTL Decreased	ΔNTL (Percentage)
China	9006	4013 (44.56%)	4933 (55.44%)	−5.19%
United States	18,980	5828 (30.71%)	13,152 (69.29%)	−2.51%
Japan	1051	211 (20.08%)	840 (79.92%)	−9.97%
India	11,731	3580 (30.52%)	8151 (69.48%)	−10.13%
Europe	19,413	5322 (24.41%)	14,091 (75.59%)	−11.39%

For India, the overall brightness of NTL decreased by 10.13%, and the regions with brightness increasing account for 30.52%, whereas those with decreasing brightness account for 69.48% (Table 2). The areas where brightness was severely decreased were mainly distributed in the interior of northern India (Uttar Pradesh, Bihar, and West Bengal) and the western coastal areas (west of Maharashtra). In the south (Tamil Nadu), northwest (parts of Punjab and Rajasthan), and central inland area (northern Andhra Pradesh), the decreased brightness level was relatively moderate.

For the United States, the overall brightness of NTL decreased by 2.51%. The regions with a brightness increase account for 30.71% whereas those with a decrease account for 69.29% (Table 2). The areas with severely decreased brightness were mainly located in the eastern part of the United States, and some western regions also exhibited decreased brightness trends (Figure 4A). Clearly, the majority region of the United States represented decreased NTL trends, especially in the eastern areas, whereas some regions, including the Boston-Washington urban agglomeration on the east coast, the San Diego-San Francisco urban agglomeration on the west coast, the Chicago-Pittsburgh urban agglomeration on the coast of the Great Lakes in the north, and the central urban agglomeration, exhibited increased NTL features (Kansas City, Dallas-Fort Worth urban agglomeration). Interestingly, although the NTL radiance in the periphery of the urban agglomeration was decreased, the NTL radiance in the inner area of these urban agglomerations was increased.

For Japan, the overall brightness of NTL decreased by 9.97%. The regions with increased NTL radiance account for 20.08% and those with decreased radiance account for 79.92% (Table 2). The areas with decreased radiance were mainly located on Kyushu Island, Shikoku Island, Honshu Island, and Hokkaido (Figure 4A). For example, the NTL radiance of the three major urban agglomerations on the island of Honshu, including the Tokyo urban agglomeration, the Osaka urban agglomeration, and the Nagoya urban agglomeration, mainly presented decreased brightness characteristics. In contrast, a few areas on the fringe of the Osaka urban agglomeration and the Nagoya urban agglomeration represented increased brightness trends (Figure 4A).

For Europe, the NTL brightness decreased by 11.39%. The areas with increased NTL radiance account for 24.41% whereas the decreased radiance areas account for 75.59% (Table 2). The NTL radiance of main urban areas in Northern Europe, Eastern Europe, and Central Europe was mainly decreased except for some Western European and Mediterranean coastal cities such as London in the United Kingdom and Madrid in Spain (Figure 4A).

The NTL in South America and Africa decreased by 4.44% and 8.35%, respectively (Figure 4A), whereas the overall decreased trends were not as pronounced as in the above-mentioned parts of the world.

3.3. Calibrating and Mapping ΔGDP

Cross-validation was introduced to evaluate the precision of the GWR model using R^2, RMSE, and MAE, respectively. Clearly, there is a significant positive linear correlation between ΔNTL and ΔGDP at the national scale, and the R^2, RMSE, and MAE were 0.7735, 66.2612 (billions of USD), and 31.6523 (billions of USD), respectively (Figure 5a). Meanwhile, the actual ΔGDP obtained from the International Monetary Fund (IMF) was used to validate the predicted ΔGDP calibrated by the GWR model. The results showed the precision was acceptable with R^2 = 0.6707, RMSE = 105.1068, and MAE = 28.5157, respectively (Figure 5b). Moreover, the *t*-test was conducted to verify the difference between actual ΔGDP and predicted ΔGDP (Table 3), and the results of the *t*-test are presented in the Appendix A (Tables A1 and A2).

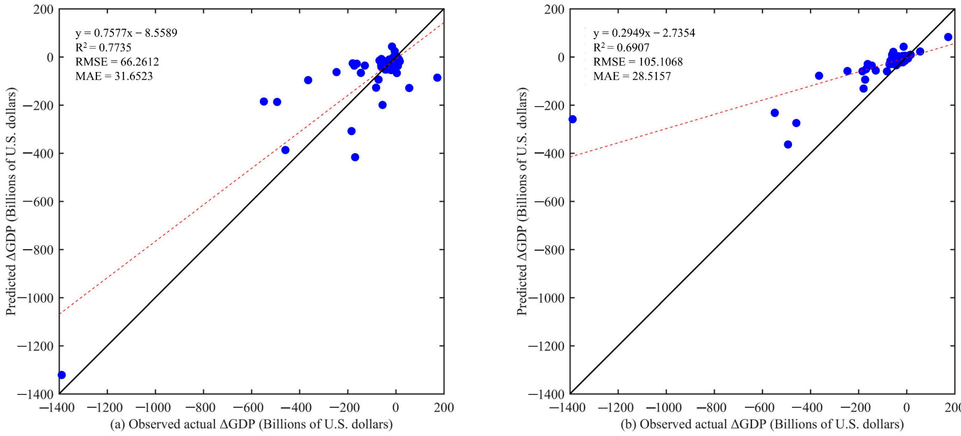

Figure 5. The scatter plots of GWR model fitting (**a**) and model validating (**b**).

Table 3. Paired Samples Statistics.

Pair 1	Mean	N	Std. Deviation	Std. Error Mean
ΔGDP	−40.74895810	151	139.553830153	11.356729636
ΔGDP_i	−39.43238498	151	120.223505126	9.783650094

3.4. Determining the ΔGDP by the GWR Model

The ΔGDP demonstrated decreased trends in most regions all over the world during the COVID-19 pandemic, and the world economy has been seriously affected and has fallen into stagnation and recession (Figure 4B).

For China, the GDP decreased by 3.36%, and the areas with increased GDP account for 36.31% but the areas with a decrease account for 63.69% (Table 4). The significant differences of the ΔGDP could also be divided by the Hu line. The GDP changes mainly accumulated east of the Hu line, whereas west of the Hu Line, the ΔGDP was not remarkable, especially in Tibet and Qinghai. Specifically, the main GDP reduction areas were distributed in the north of China, the central part of China especially Hubei province, and the eastern part of China (Figure A1 (China, d–f)). In contrast, three main urban agglomerations including the Beijing-Tianjin-Hebei, the Yangtze River Delta, and the Pearl River Delta represented features of sporadically increased GDP (Figure A1 (China, a–c)).

Table 4. The variation of GDP due to the COVID-19 pandemic.

Location	Area with Increased GDP (Grids and Proportion)	Area with Decreased GDP (Grids and Proportion)	Total GDP Change (Billions of USD)	Total GDP Change (Percentage)
China	3272 (36.31%)	5739 (63.69%)	−548.50	−3.36%
United States	5870 (30.90%)	13,125 (69.1%)	−1389.01	−6.22%
Japan	24 (2.28%)	1027 (97.72%)	−364.362	−6.73%
India	3258 (27.76%)	8478 (72.24%)	−493.41	−15.41%
Europe	2057 (10.88%)	16,844 (89.12%)	−1117.02	−5.09%

For India, the GDP reduced by −15.41%, and the areas with increased GDP account for 27.76% but the areas with a decrease account for 72.24% (Table 4). The significant GDP reduction areas were mainly located in the interior of northern India (Uttar Pradesh, Bihar, West Bengal) and the western coastal areas (west of Maharashtra). In the south (Tamil Nadu), northwest (parts of Punjab and Rajasthan), and central inland area (northern Andhra Pradesh), the decrease level was relatively moderate (Figure A1 (India, d–f)). In contrast, partial regions of India demonstrated increased trends, including the rural areas of the northwest and west of New Delhi, and the rural areas of central and south India such as Chennai, Mumbai, New Delhi, etc. (Figure A1 (India, a–c)).

For the United States, the GDP decreased by 6.22%. The areas with increased GDP account for 30.90% and the areas with a decrease account for 69.1% (Table 4). Although parts of western regions such as Salt Lake City, Seattle, and Meridian represented decreased GDP trends, the majority of areas showing a decrease were distributed in the eastern part of the country (Figure A1 (United States)). In contrast, some urban agglomerations including Boston-Washington on the east coast, San Diego-San Francisco on the west coast, and Chicago-Pittsburgh on the coast of the Great Lakes in the north exhibited increased GDP features (Figure A1 (United States, a,c,d,f)).

For Japan, the GDP decreased by 6.73%. The areas with increased GDP account for 2.28% and the areas showing a decrease account for 97.72% (Table 4). Clearly, the decreased GDP trends were the prominent characteristic of the entire country (Figure A2 (Japan, e)). The sporadic increased GDP areas were mainly distributed in the major urban agglomerations such as Tokyo, Osaka, Nagoya, Sapporo, and Fukuoka (Figure A2 (Japan, a–d,f)).

For Europe, the GDP decreased by 5.09%. The increased GDP areas account for 10.88% whereas the decreased GDP areas account for 89.12% (Table 4). Even though a few countries such as Ireland and some European cities including London, Birmingham, and Madrid had increased GDP, the decreased GDP trends were the dominant characteristic across the entirety of Europe. The GDP in the metropolitan areas of Europe such as Paris, Berlin, Moscow, St. Petersburg, and Warsaw showed slightly increasing trends (Figure A2 (Europe, a–f)).

For South America, GDP decreased by 9.8%. The decrease happened in the majority of regions except for Porto Alegre and São Paulo in Brazil, and Asuncion, the capital of Paraguay.

For Africa, GDP decreased by 3.23%. Further observations showed that the GDP in the south of the Sahara decreased except for Pretoria in South Africa. In contrast, the GDP of Egypt demonstrated increasing trends (Figure 4B).

4. Discussion

4.1. Evaluation of GM(1, 1) in Predicting NTL Image

Earth's artificially lit outdoor area increased by 2.2% from 2012 to 2016, with a total radiance growth of 1.8% yearly. Overall, the radiance of regions lit higher than 5 nw/cm/sr grew by 1.8% yearly globally [41]. Specifically, some of the world's brightest regions, such as Italy, Netherlands, Spain, and the United States were relatively stable. In addition, some developing countries including South America, Africa, and Asia revealed an increasing trend in nighttime lights [42]. In contrast, a small number of countries such as Yemen and Syria are experiencing warfare, which led to a decreasing trend in nighttime lights [25]. Obviously, the NTL exhibits a relatively stable changing trend according to the above literature. Meanwhile, the NTL was remarkably influenced by the pandemic which can be regarded as a grey system [35]. Therefore, the GM(1, 1) model is suitable for simulating NTL under the assumption of no epidemic.

Obviously, the performance of GM(1, 1) in predicting the NTL in 2019 at the national scale is better than on the grid scale according to the present study. The possible reasons are analyzed and listed below. The relative lower precision at the grid scale is mainly because each pixel may have a slight positive or negative bias through the predicted process and these biases were simultaneously summarized once. The lower precision may be generated by the accumulation of biases [35]. Positive and negative biases are offset resulting in a higher precision at the country scale. Therefore, using the global NTL images from 2013 to

2019 combined with the GM(1, 1) model to simulate the NTL image assuming that there was no pandemic in 2020 is reliable in the present study.

4.2. Variation Characteristics of Global GDP

It is widely known that 94% of the population and 96% of the GDP of China is mainly distributed east of the Hu line [40,43]. Although the area west of the Hu line of China accounts for 44% of the area of China, the population and GDP only account for 6% and 4%. Therefore, the GDP variations east of the Hu line are more significant on the west side. Additionally, COVID-19 broke out in December 2019, which overlapped with the Lunar New Year holiday [43], which led to human and economic activities in urban areas representing a decreasing trend because plenty of urban residents returned to their hometowns to celebrate the Lunar New Year [7,33]. Meanwhile, a first-level public health emergency response was carried out by several provinces in China and a series of social and economic activities were suspended on 23 January 2020 to prevent the spread of the pandemic, which seriously affected GDP and led to a significant GDP reduction in the northern, central, and eastern parts of China. The GDP of Hubei province suffered the most serious influence due to the tough restrictions implemented by the local authorities [34].

In India, the situations were similar, and the lockdown suspended industries, the traffic system, and normal work routines [44]. The differences lie in the urbanization rate, which is only 34.93%. This means a larger population lives in rural areas when compared with China. It was reported that the NTL brightness significantly increased in the surrounding areas of Delhi, Mumbai, and Kolkata after the lockdown, possibly because of the urban residents' return to their hometowns [32]. Thus, areas with decreasing GDP were mainly distributed within the cities, whereas regions with increasing GDP were located in suburban areas. Moreover, economic activities in northern India (Uttar Pradesh, Bihar) and northeastern India (West Bengal) far from urban agglomerations were seriously affected by the pandemic during the national lockdown. Hence, GDP in most of the north and northeast of India has suffered a serious decrease (Figures 4B and A1).

For the United States, travel from China was restrained on 30 January 2020, and then a series of restrictions was implemented for preventing the rapid increase in COVID-19 cases, including social distancing orders, shelter-in-place orders, school closures, and travel restrictions. These restrictions led to a sharp decrease in human activities [45]. Interestingly, the GDP of the inner area in the urban agglomeration increased but in the surrounding areas it decreased during the spreading of COVID-19. The possible reasons were as follows. Firstly, the urbanization rate of the United States is up to 82.66% and a larger population lives in cities [46]. The NTL of the United States demonstrated that the majority of people who live in urban areas did not move to suburban areas for shelter. Secondly, the attitude toward COVID-19 of the residents in the United States was completely different from that in Asia and the policies implemented by the local authorities were relatively flexible. Therefore, the main industries, even though they were affected, were still running during the pandemic. In contrast, GDP in the vast western and eastern inland areas was greatly reduced which was in line with the decreasing trends of NTL radiance obtained by Section 3.2 of this study. The capacity for reduction in risks from phenomena such as pandemics in small and medium cities in the U.S. was significantly weaker than in urban agglomerations [43].

In contrast, most European countries started a lockdown policy at the end of March 2020, and Japan did so in mid-April 2020. During the national lockdown, nearly all industrial activities were suspended in these countries, thus that the economy suffered a serious hit during the epidemic. NTL and GDP decreased in Europe and Japan due to lockdown restrictions. The highly industrialized open economies of Japan and most European countries, occupying the high end of the international value chain and having a high degree of external dependence, were susceptible to suffering a huge shock owing to the spreading of the pandemic infection globally [47]. The urbanization rate of Japan and Europe is about 93.02% and 72.54%, respectively. Although people stayed at home and refrained from non-essential travel, the regional economic resilience was low and the economy suffered a serious influence owing to the limited resources during the lockdown [43].

4.3. The Relationship between ΔGDP and COVID-19 Infection Rate

Did the COVID-19 infection rate affect ΔGDP directly? We found that ΔGDP has no direct relation to the COVID-19 infection rate (Figure 6a), but the prevention and control measures caused changes in human activities that led to variations in GDP [31–33]. Figure 4B demonstrates that most countries suffered decreased GDP trends and the COVID-19 infection rate had no linear relation with ΔGDP. However, at the country scale, the ΔGDP is significantly correlated with the Governmental Response Stringency Index [5,48], an indicator of the severity of government lockdown measures to slow the transmission of COVID-19 (Figure 6b). It is noted that some countries presenting a positive ΔGDP or experiencing warfare were excluded for avoiding outliers (Figure 6b).

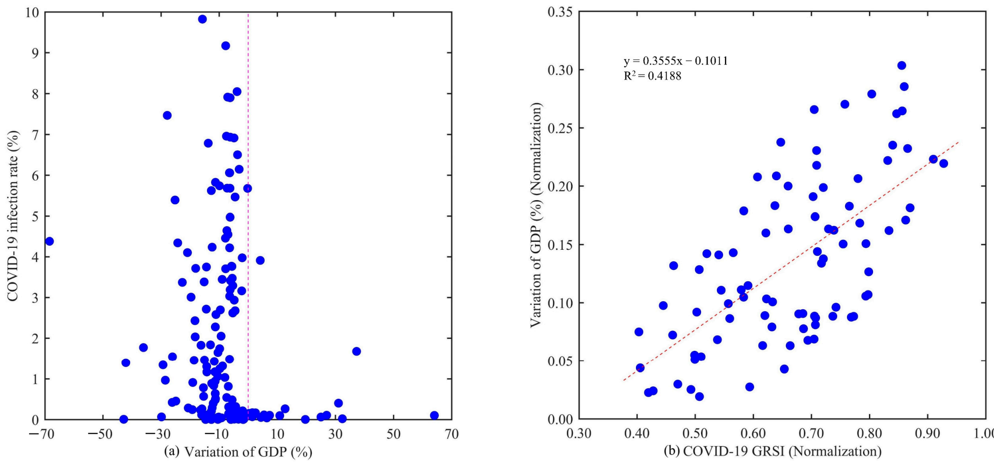

Figure 6. The relationship between COVID-19 infection rate and ΔGDP rate (**a**). The relationship between the COVID-19 Government Response Stringency Index (GRSI) and ΔGDP rate (**b**). Note: A GRSI with a value from 0 to 100 (100 = strictest) was surveyed according to nine response indicators including travel bans, school closures, and workplace closures [5,48]. The GRSI was rescaled to 0–1 for unit consistency with the variation of GDP in the present study.

4.4. The Possible Reasons for Countries Having Positive GDP Growth during the Spread of COVID-19

It was reported that the global economy was ravaged by the COVID-19 pandemic in 2020 [1–5]. However, several countries, including Iran, Afghanistan, Egypt, Côte d'Ivoire, Vietnam, Myanmar, South Korea, and Ireland kept an increasing trend in GDP (Figure 7). Specifically, it was inferred that the GDP of South Korea would drop by 1.23% in 2020 according to IMF-projected GDP data; however, the actual GDP of South Korea only reduced by 1% in 2020 (Tables 5 and 6) even though it was troubled by the virus at the beginning of the year [12]. It is also noted that the public health system of South Korea was considered a model of COVID-19 infection prevention. South Korea never carried out a complete national lockdown, i.e., borders were not thoroughly closed down, and most of the businesses kept running [47]. Therefore, South Korea's GDP decreased less than the prediction by IMF.

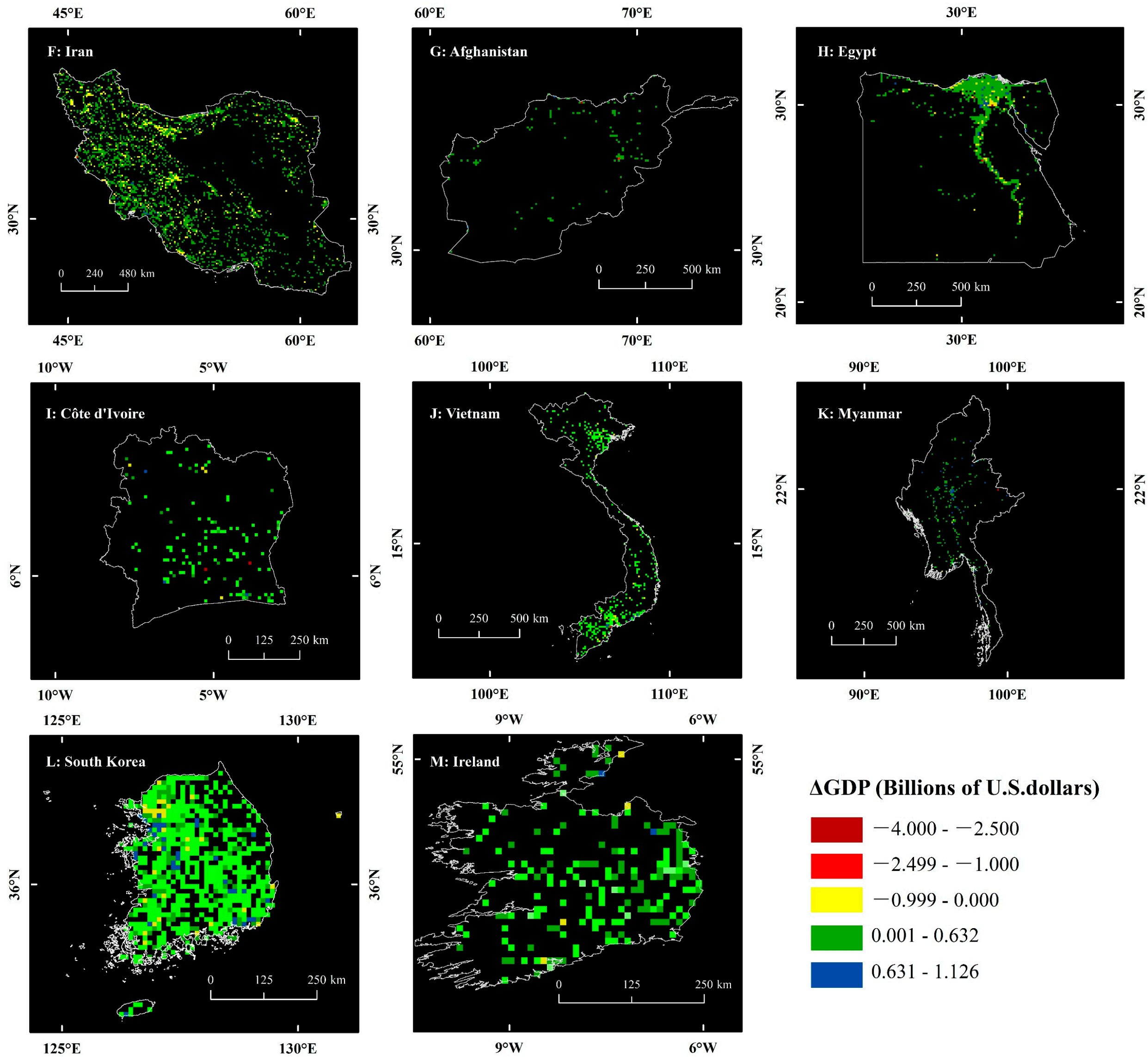

Figure 7. The 0.1° × 0.1° resolution map of countries with positive ΔGDP in 2020.

Table 5. Actual GDP and Projected GDP in 2020.

Location	Actual GDP in 2020 (Billions of USD)	Projected GDP for 2020 (Billions of USD)	ΔGDP (Billions of USD)
South Korea	1630.87	1626.55	4.32
Iran	635.72	463.08	172.64
Myanmar	81.26	72.11	9.15
Vietnam	340.82	284.85	55.97
Ireland	418.72	402.05	16.67
Côte d'Ivoire	61.40	48.35	13.05
Egypt	361.85	353.00	8.85
Afghanistan	19.81	18.86	0.95

Note: the data were made available by the IMF.

Meanwhile, warnings from China in early January 2020 concerning COVID-19 prompted responses in Southeast Asian countries such as Vietnam and Myanmar (Figure 7). Vietnam is one of the few countries where the COVID-19 pandemic was controlled by the end of 2020 [12]. Severe outcomes were aborted due to timely protection and restrictions on travel. The GDP growth of Southeast Asian countries varied from 2.9% (in Vietnam) to 3.2% (in

Myanmar) benefiting from prompt response measures (Tables 5 and 6). Moreover, in 2020, a large number of foreign companies entered Myanmar to invest. To assure economic growth, maintaining growth in imports and exports was one of the important measures in Vietnam. According to statistics for 2020, the total import and export volume of Vietnam was about 543.9 billion USD, a year-on-year increase of 5.1%, achieving a surplus of 19.10 billion USD. Hence, the ΔGDP of Vietnam and Myanmar was positive in 2020 [49].

Table 6. Actual GDP growth rate and projected GDP growth rate in 2020.

Location	Actual GDP Growth Rate in 2020 (%)	Projected GDP Growth Rate for 2020 (%)
South Korea	−1.00	−1.23
Iran	1.50	−20.33
Myanmar	3.20	−8.42
Vietnam	2.90	−13.56
Ireland	2.50	0.92
Côte d'Ivoire	2.30	−17.40
Egypt	3.60	1.06
Afghanistan	2.67	−2.23

Note: the data were made available by the IMF.

For Iran, the GDP in 2020 was expected to decrease by 20.33% according to IMF-inferred GDP data. However, Iran's actual exports were increased by 24.41%, and imports raised by 7.53% in 2020, due to the increase in import and export trade. In addition, compared with the months before the pandemic, transaction volume increased by 12% year-on-year according to electronic payment and online terminal consumption data after the national lockdown ended [50]. Hence, despite the impact of the COVID-19 pandemic, the real GDP of Iran rose by 1.5% in 2020 (Tables 5 and 6) (Figure 7).

For Egypt, the actual GDP increased by 3.60% in 2020, which was higher than the IMF prediction (1.06%) (Table 6). A series of flexible anti-epidemic policies were adopted by the Egyptian government to prevent a pandemic, and ensure economic development [12,51]. Moreover, several financial and material resources were invested in various aspects by the government to stimulate economic development. For example, 100 billion EGP were allocated by the central bank to prevent the epidemic from spreading, to cut the prices of electricity and gas, and to supply support for the real estate industries and tourism [51]. Thus, the ΔGDP of Egypt was 8.85 billion USD higher than predicted (Table 6 and Figure 7).

Ireland had urged multinational corporations to construct factories through tax reduction before the pandemic outbreak. Lots of large technology companies have established regional headquarters in Ireland, such as Facebook, and Google's parent company. In addition, pharmaceutical companies, such as Pfizer and Merck, have established large manufacturing plants. The demand for medicines, digital services, and equipment such as video communications has largely increased during the COVID-19 pandemic, which has increased Irish merchandise exports, hitting a record high in 2020 [52]. Thus, the GDP growth of Ireland in 2020 was higher than expected (Figure 7) (Tables 5 and 6).

Afghanistan is experiencing continuous wars and armed conflicts that have led to tremendous damage over most of the past two decades. The GDP of Afghanistan was predicted to decrease by 2.23% in 2020 according to IMF forecasts (Tables 5 and 6). Fortunately, a peace deal between the US and the Taliban was achieved in February 2020. Moreover, armed groups announced ceasefires to support responses to COVID-19. Overall, armed conflict events (battles and explosions) in Afghanistan obviously declined during the first months of the COVID-19 pandemic [53]. The economy of Afghanistan obtained a rare opportunity and recovered to a certain extent in 2020 (Figure 7).

Côte d'Ivoire is one of the largest economies in West Africa. It mainly depends on agriculture production [54]. Nearly one-fifth of its GDP is generated by primary industry. For example, Côte d'Ivoire is one of the world's largest cocoa producers and exporters accounting for 30% of world production, one of the world's top three cashew nut producers and exporters, and an important exporter of palm oil, coffee, and petroleum [55]. Clearly, Côte d'Ivoire received few impacts during the COVID-19 pandemic due to the agricultural economy feature (Figure 7), which ensured its actual GDP increased by 2.3% in 2020 (Tables 5 and 6).

In addition, quantitative analysis between GDP and influencing factors for some countries are presented in the Supplementary Materials (Tables S1 and S2, and Figures S1 and S2).

4.5. Limitation

In spite of the merits of the current work, some limitations need to be addressed in the future. Firstly, the reliability of the GM(1, 1) model in estimating NTL images should be further evaluated. Although the GM(1, 1) model is considered a versatile forecasting model and the NTL has a significant positive correlation with socioeconomic variables including GDP, urban area, and population density [56], random disturbances are not conducive to grey modeling. Actually, the NTL radiance in some regions of the world is changing but not stable. A rather large random disturbance can reduce the forecast accuracy of the GM(1, 1) model [35]. Secondly, the capacity of NTL in estimating primary industry is weak. The contribution of the agricultural sector was not fully considered when NTL images were used for estimating GDP spatial distribution [57]. In the current study, the primary industry GDP was not distinguished from the national GDP statistics data. Thus, the estimation accuracy needs further improvement in the future. Nighttime light appears to be an unstable phenomenon in some minority areas due to war or other sudden events, equivalent to outliers. However, nighttime light is relatively stable in most parts of the world. Thirdly, country-level GDP data were introduced to research on a global scale due to the availability of data. Although the GWR model is a local model that can be used to reflect the spatial heterogeneity of GDP at the country scale, there are still some shortcomings in capturing geographic differences within countries with larger areas. Fourthly, the inner mechanism for GDP is complicated. To our knowledge, GDP is not only affected by natural factors but also impacted by anthropic factors. In addition, GDP may be influenced by some uncontrollable factors such as welfare, trade war, and sanctions. Though GDP was seriously impacted by the COVID-19 pandemic all over the world, the policies and measures were the most important affecting factors for GDP. For example, it was reported that timing and the stringency of lockdown policies were endogenous to the economy during the pandemic. The spatiality of transmission, immunity of humans, qualities of healthcare systems, the effectiveness of state policy/measure, and vaccination coverage rates were completely different in each nation, which led to the consequences of subsequent socio-economic situations differing during the COVID-19 pandemic [58]. Additionally, countries had different schemes for testing and reporting COVID-19 cases. For example, extensive testing for COVID-19 was done by some countries but not others. Our results may have some uncertainties and biases. Fifthly, the GDP of 151 countries including actual GDP and predicted GDP used in the present were obtained from the IMF. The quality and precision of the IMF GDP may exist as uncertainties due to a lack of effective evaluation and external validation. Meanwhile, the assessment for the $0.1 \times 0.1^{\circ}$ resolution maps of GDP variation globally obtained from the current study was inadequate owing to few global grid-scale GDP products existing. To address the above issues, we plan to comprehensively consider the potentially influential factors for GDP, and put more affecting factors into consideration for estimating GDP. Moreover, to improve the accuracy of GDP predicted via NTL images, the secondary and tertiary industry production will be inferred by NTL images, and the primary industry production is planned to be calculated based on the land use/cover data [57]. Furthermore, fine scales such as states, prefectures, and provinces will be introduced to the study if the data availability can be solved in the future. Machine learning models may be considered to infer GDP globally on the grid scale to promote precision [59].

5. Conclusions

This study proposed a new perspective regarding the impacts of the global COVID-19 pandemic on socio-economic activities. The GM(1, 1) model was introduced to infer simulated NTL (SNTL) images under the assumption that there was no COVID-19 epidemic in 2020, and the ΔNTL was obtained by actual observed NTL deducting SNTL. Furthermore, the ΔGDP was calculated by actual statistical GDP data deducting predicted GDP data at the country scale. The GWR was introduced to quantitatively determine the relation between ΔGDP and ΔNTL at the country scale. Finally, the distribution of the ΔGDP was mapped using the GWR model globally at $0.1° \times 0.1°$ resolution in 2020. Some interesting results were achieved. First, the GM(1, 1) model can be used to predict NTL images based on historical NTL images, and the prediction accuracy of the GM(1, 1) model in estimating NTL images globally was acceptable. Second, the NTL in the majority of world decreased but some minority areas exhibited increased trends. The ANTL brightness in 2020 decreased by 8.28% compared with the SNTL in 2020 simulated under the assumption that there was no COVID-19 pandemic. The NTL of major economies across six continents was significantly affected by the COVID-19 pandemic to some extent. Third, there is a significant positive linear correlation between ΔNTL and ΔGDP at the national scale, and the R^2, RMSE, and MAE were 0.7735, 66.2612, and 31.6523, respectively. The GWR model combined with ΔNTL can be used to map the ΔGDP at the grid scale globally. The ΔGDP demonstrated decreased trends in most regions all over the world during the spread of the COVID-19 pandemic in 2020, and the world economy has been seriously affected, falling into stagnation and recession. The methods used in this paper can supply a scientific basis for determining the effects of the COVID-19 pandemic on GDP and an effective and fast method for mapping variation of GDP at a grid scale globally. The outcomes of the present study can be used for policy decision-making and loss assessment owing to the COVID-19 pandemic.

Supplementary Materials: The following supporting information can be downloaded at: https://www.mdpi.com/article/10.3390/su142215201/s1.

Author Contributions: Conceptualization: B.G.; Methodology: B.G.; Investigation: W.Z.; Visualization: W.Z.; Funding acquisition: B.G.; Project administration: W.D.; Supervision: B.G. and P.L.; Writing—original draft preparation: B.G., W.Z. and L.P.; Writing—review and editing: B.G., W.Z., X.Z. and L.P. All authors have read and agreed to the published version of the manuscript.

Funding: This work was supported by the Natural Science Foundation of Shaanxi Province (2021JM-388), and Fundamental Research Funds for the Central Universities, CHD (300102352505).

Institutional Review Board Statement: Not applicable.

Informed Consent Statement: All the participants were given an informed consent to be signed upon they consented to participate in this study.

Data Availability Statement: The data presented in this study are available on request from the corresponding author. The data are not publicly available due to privacy considerations.

Acknowledgments: We are grateful to Dingming Zhang, Bo Zhang, Yan Wang, and Yi Bian for editing the manuscript.

Conflicts of Interest: The authors declare that they have no competing interests. The content is solely the responsibility of the authors and does not necessarily represent any official views.

Appendix A

Table A1. Paired Samples Correlations.

		N	Correlation	Sig.
Pair 1	ΔGDP & ΔGDP_i	151	0.879	0.000

Table A2. Paired Samples Test.

		Paired Differences					t	df	Sig. (2-Tailed)
		Mean	Std. Deviation	Std. Error Mean	95% Confidence Interval of the Difference				
					Lower	Upper			
Pair 1	$\Delta GDP - \Delta GDP_i$	−1.317	66.469	5.410	−12.005	9.371	−0.243	150	0.808

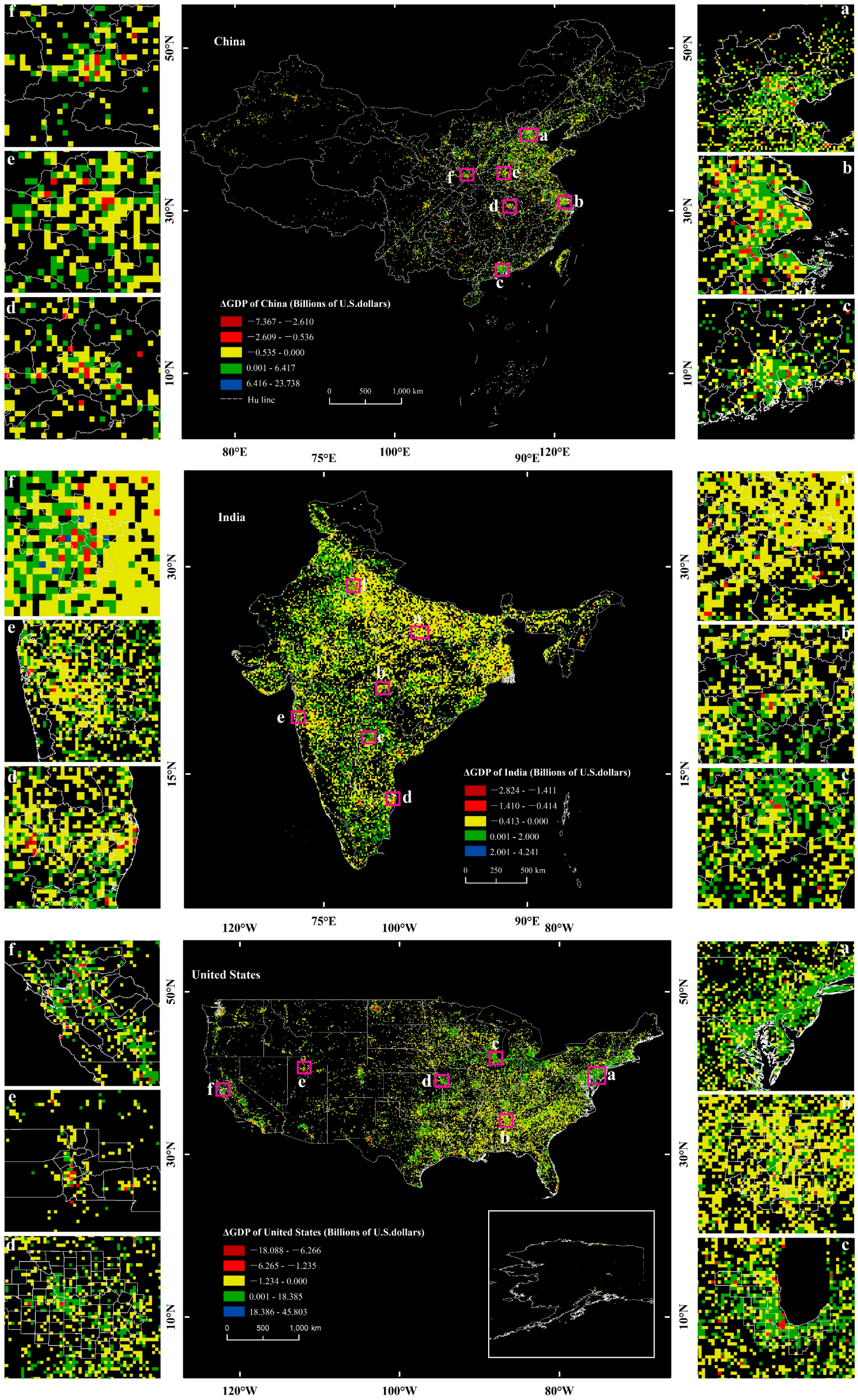

Figure A1. The 0.1° × 0.1° resolution ΔGDP map of China, India, and the United States in 2020.

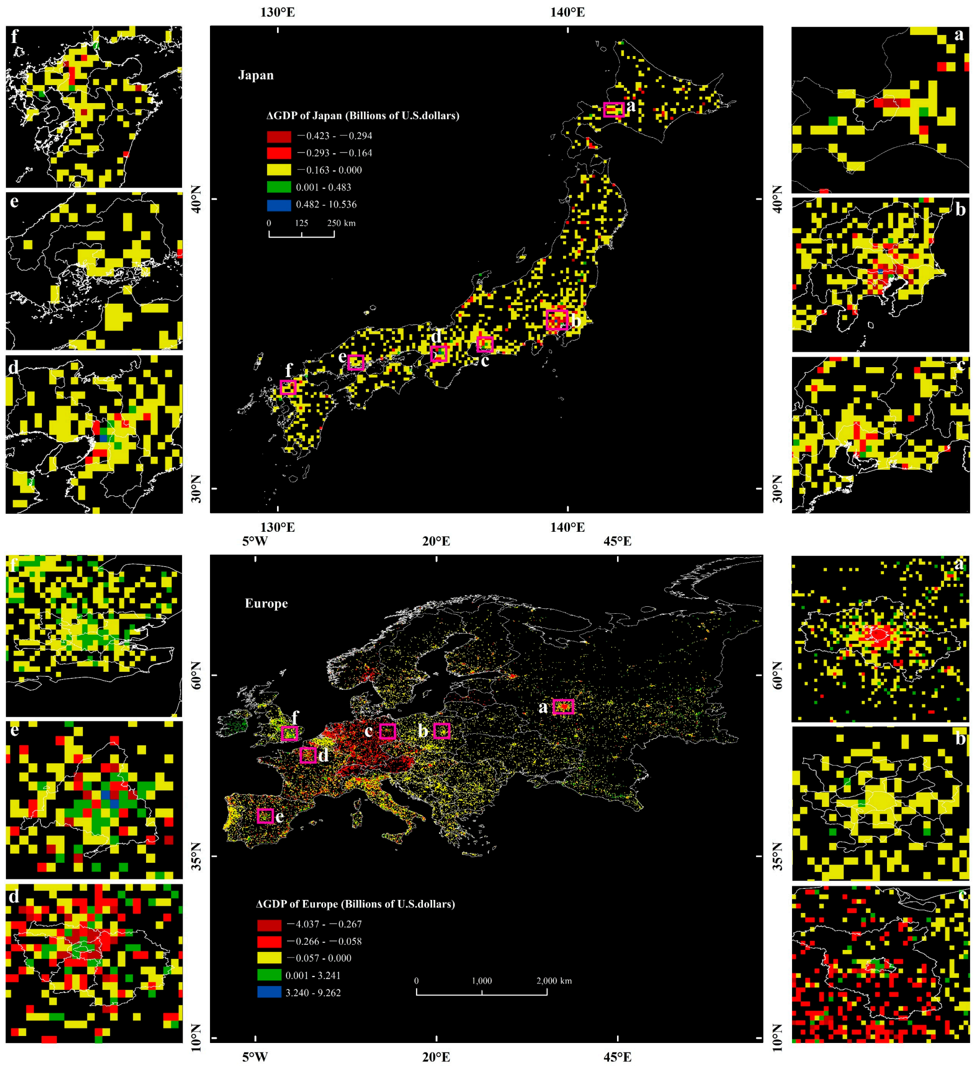

Figure A2. The 0.1° × 0.1° resolution ΔGDP map of Japan and Europe in 2020.

References

1. Dong, E.; Du, H.; Gardner, L. An interactive web-based dashboard to track COVID-19 in real time. *Lancet Infect. Dis.* **2020**, *20*, 533–534. [CrossRef]
2. Center for Systems Science and Engineering (CSSE) at Johns Hopkins University (JHU). Available online: https://coronavirus.jhu.edu/map.html (accessed on 1 February 2022).
3. Saraswat, R.; Saraswat, D.A. Research opportunities in pandemic lockdown. *Science* **2020**, *368*, 594–595. [CrossRef]
4. Lai, S.; Ruktanonchai, N.W.; Zhou, L.; Prosper, O.; Luo, W.; Floyd, J.R.; Wesolowski, A.; Santillana, M.; Zhang, C.; Du, X.; et al. Effect of non-pharmaceutical interventions to contain COVID-19 in China. *Nature* **2020**, *585*, 410–413. [CrossRef] [PubMed]
5. Miyazaki, K.; Bowman, K.; Sekiya, T.; Takigawa, M.; Neu, J.L.; Sudo, K.; Osterman, G.; Eskes, H. Global tropospheric ozone responses to reduced NOx emissions linked to the COVID-19 worldwide lockdowns. *Sci. Adv.* **2021**, *7*, eabf7460. [CrossRef] [PubMed]
6. Pei, L.; Wang, X.; Guo, B.; Guo, H.; Yu, Y. Do air pollutants as well as meteorological factors impact Corona Virus Disease 2019 (COVID-19)? Evidence from China based on the geographical perspective. *Environ. Sci. Pollut. Res.* **2021**, *28*, 35584–35596. [CrossRef] [PubMed]
7. Su, F.; Fu, D.; Yan, F.; Xiao, H.; Pan, T.; Xiao, Y.; Kang, L.; Zhou, C.; Meadows, M.; Lyne, V.; et al. Rapid greening response of China's 2020 spring vegetation to COVID-19 restrictions: Implications for climate change. *Sci. Adv.* **2021**, *7*, eabe8044. [CrossRef]
8. Chossiere, G.P.; Xu, H.; Dixit, Y.; Isaacs, S.; Eastham, S.D.; Allroggen, F.; Speth, R.L.; Barrett, S.R.H. Air pollution impacts of COVID-19-related containment measures. *Sci. Adv.* **2021**, *7*, eabe1178. [CrossRef]
9. Laborde, D.; Martin, W.; Swinnen, J.; Vos, R. COVID-19 risks to global food security. *Science* **2020**, *369*, 500–502. [CrossRef]
10. Hammer, M.S.; van Donkelaar, A.; Martin, R.V.; McDuffie, E.E.; Lyapustin, A.; Sayer, A.M.; Hsu, N.C.; Levy, R.C.; Garay, M.J.; Kalashnikova, O.V.; et al. Effects of COVID-19 lockdowns on fine particulate matter concentrations. *Sci. Adv.* **2021**, *7*, eabg7670. [CrossRef]

11. Stokstad, E.; Aridi, R. Pandemic lockdown stirs up ecological research. *Science* **2020**, *369*, 893. [CrossRef]
12. International Moetary Fund. Available online: https://www.imf.org/en/Home (accessed on 1 April 2021).
13. Coccia, M. The relation between length of lockdown, numbers of infected people and deaths of COVID-19, and economic growth of countries: Lessons learned to cope with future pandemics similar to Covid-19 and to constrain the deterioration of economic system. *Sci. Total Environ.* **2021**, *775*, 145801. [CrossRef]
14. Livingston, G.; Huntley, J.; Sommerlad, A.; Ames, D.; Ballard, C.; Banerjee, S.; Brayne, C.; Burns, A.; Cohen-Mansfield, J.; Cooper, C.; et al. Dementia prevention, intervention, and care: 2020 report of the Lancet Commission. *Lancet* **2020**, *396*, 413–446. [CrossRef]
15. Brouwer, P.J.M.; Caniels, T.G.; van der Straten, K.; Snitselaar, J.L.; Aldon, Y.; Bangaru, S.; Torres, J.L.; Okba, N.M.A.; Claireaux, M.; Kerster, G.; et al. Potent neutralizing antibodies from COVID-19 patients define multiple targets of vulnerability. *Science* **2020**, *369*, 643–650. [CrossRef] [PubMed]
16. Mercader-Moyano, P.; Morat, O.; Serrano-Jimenez, A. Urban and social vulnerability assessment in the built environment: An interdisciplinary index-methodology towards feasible planning and policy-making under a crisis context. *Sustain. Cities Soc.* **2021**, *73*, 103082. [CrossRef]
17. Tan, X.; Zhu, X.; Chen, J.; Chen, R. Modeling the direction and magnitude of angular effects in nighttime light remote sensing. *Remote Sens. Environ.* **2022**, *269*, 112834. [CrossRef]
18. Macinko, J.A.; Shi, L.; Starfield, B. Wage inequality, the health system, and infant mortality in wealthy industrialized countries, 1970–1996. *Soc. Sci. Med.* **2004**, *58*, 279–292. [CrossRef]
19. Feng, Y.; Wang, X. Effects of National New District on economic development and air pollution in China: Empirical evidence from 69 large and medium-sized cities. *Environ. Sci. Pollut. Res.* **2021**, *28*, 38594–38603. [CrossRef] [PubMed]
20. Huang, Z.; Li, S.; Gao, F.; Wang, F.; Lin, J.; Tan, Z. Evaluating the performance of LBSM data to estimate the gross domestic product of China at multiple scales: A comparison with NPP-VIIRS nighttime light data. *J. Clean. Prod.* **2021**, *328*, 129558. [CrossRef]
21. Guo, B.; Zhang, D.; Pei, L.; Su, Y.; Wang, X.; Bian, Y.; Zhang, D.; Yao, W.; Zhou, Z.; Guo, L. Estimating PM2.5 concentrations via random forest method using satellite, auxiliary, and ground-level station dataset at multiple temporal scales across China in 2017. *Sci. Total Environ.* **2021**, *778*, 146288. [CrossRef]
22. Wang, X.; Sutton, P.C.; Qi, B. Global Mapping of GDP at 1 km^2 Using VIIRS Nighttime Satellite Imagery. *ISPRS Int. J. Geo-Inf.* **2019**, *8*, 580. [CrossRef]
23. Bennett, M.M.; Smith, L.C. Advances in using multitemporal night-time lights satellite imagery to detect, estimate, and monitor socioeconomic dynamics. *Remote Sens. Environ.* **2017**, *192*, 176–197. [CrossRef]
24. Zheng, Q.; Weng, Q.; Wang, K. Developing a new cross-sensor calibration model for DMSP-OLS and Suomi-NPP VIIRS night-light imageries. *ISPRS-J. Photogramm. Remote Sens.* **2019**, *153*, 36–47. [CrossRef]
25. Li, X.; Li, D.; Xu, H.; Wu, C. Intercalibration between DMSP/OLS and VIIRS night-time light images to evaluate city light dynamics of Syria's major human settlement during Syrian Civil War. *Int. J. Remote Sens.* **2017**, *38*, 5934–5951. [CrossRef]
26. Gao, S.; Chen, Y.; Liang, L.; Gong, A. Post-Earthquake Night-Time Light Piecewise (PNLP) Pattern Based on NPP/VIIRS Night-Time Light Data: A Case Study of the 2015 Nepal Earthquake. *Remote Sens.* **2020**, *12*, 2009. [CrossRef]
27. Liu, C.; Lin, J.; Moslin, R.; Tokarski, J.S.; Muckelbauer, J.; Chang, C.; Tredup, J.; Xie, D.; Park, H.; Li, P.; et al. Identification of Imidazo 1,2-b pyridazine Derivatives as Potent, Selective, and Orally Active Tyk2 JH2 Inhibitors. *ACS Med. Chem. Lett.* **2019**, *10*, 383–388. [CrossRef]
28. Li, J.; Qiu, Y.; Cai, Y.; Zhang, K.; Zhang, P.; Jing, Z.; Wu, Q.; Ma, S.; Liu, H.; Chen, Z. Trend in fishing activity in the open South China Sea estimated from remote sensing of the lights used at night by fishing vessels. *ICES J. Mar. Sci.* **2022**, *79*, 230–241. [CrossRef]
29. Jiang, W.; He, G.; Long, T.; Guo, H.; Yin, R.; Leng, W.; Liu, H.; Wang, G. Potentiality of Using Luojia 1-01 Nighttime Light Imagery to Investigate Artificial Light Pollution. *Sensors* **2018**, *18*, 2900. [CrossRef]
30. Guo, B.; Wang, Y.; Pei, L.; Yu, Y.; Liu, F.; Zhang, D.; Wang, X.; Su, Y.; Zhang, D.; Zhang, B.; et al. Determining the effects of socioeconomic and environmental determinants on chronic obstructive pulmonary disease (COPD) mortality using geographically and temporally weighted regression model across Xi'an during 2014–2016. *Sci. Total Environ.* **2021**, *756*, 143869. [CrossRef]
31. Roberts, M. Tracking economic activity in response to the COVID-19 crisis using nighttime lights—The case of Morocco. *Dev. Eng.* **2021**, *6*, 100067. [CrossRef]
32. Ghosh, T.; Elvidge, C.D.; Hsu, F.-C.; Zhizhin, M.; Bazilian, M. The Dimming of Lights in India during the COVID-19 Pandemic. *Remote Sens.* **2020**, *12*, 3289. [CrossRef]
33. Yin, R.; He, G.; Jiang, W.; Peng, Y.; Zhang, Z.; Li, M.; Gong, C. Night-Time Light Imagery Reveals China's City Activity During the COVID-19 Pandemic Period in Early 2020. *IEEE J. Sel. Top. Appl. Earth Observ. Remote Sens.* **2021**, *14*, 5111–5122. [CrossRef]
34. Liu, Q.; Sha, D.; Liu, W.; Houser, P.; Zhang, L.; Hou, R.; Lan, H.; Flynn, C.; Lu, M.; Hu, T.; et al. Spatiotemporal Patterns of COVID-19 Impact on Human Activities and Environment in Mainland China Using Nighttime Light and Air Quality Data. *Remote Sens.* **2020**, *12*, 1576. [CrossRef]
35. Yuan, C.; Chen, D. Effectiveness of the GM(1,1) model on linear growth sequence and its application in global primary energy consumption prediction. *Kybernetes* **2016**, *45*, 1472–1485. [CrossRef]

36. Yuan, C.; Liu, S.; Fang, Z. Comparison of China's primary energy consumption forecasting by using ARIMA (the autoregressive integrated moving average) model and GM(1,1) model. *Energy* **2016**, *100*, 384–390. [CrossRef]
37. Liu, L.; Zong, H.; Zhao, E.; Chen, C.; Wang, J. Can China realize its carbon emission reduction goal in 2020: From the perspective of thermal power development. *Appl. Energy* **2014**, *124*, 199–212. [CrossRef]
38. Guo, B.; Bian, Y.; Zhang, D.; Su, Y.; Wang, X.; Zhang, B.; Wang, Y.; Chen, Q.; Wu, Y.; Luo, P. Estimating Socio-Economic Parameters via Machine Learning Methods Using Luojia1-01 Nighttime Light Remotely Sensed Images at Multiple Scales of China in 2018. *IEEE Access* **2021**, *9*, 34352–34365. [CrossRef]
39. Guo, B.; Zhang, D.; Zhang, D.; Su, Y.; Wang, X.; Bian, Y. Detecting Spatiotemporal Dynamic of Regional Electric Consumption Using NPP-VIIRS Nighttime Stable Light Data-A Case Study of Xi'an, China. *IEEE Access* **2020**, *8*, 171694–171702. [CrossRef]
40. Wu, Y.; Shi, Y.; Zhang, N.; Wang, Y.; Ren, Y. Pollution levels, characteristics, and sources of polycyclic aromatic hydrocarbons in atmospheric particulate matter across the Hu line in China. A review. *Environ. Chem. Lett.* **2021**, *19*, 3821–3836. [CrossRef]
41. Kyba, C.C.M.; Kuester, T.; Sanchez de Miguel, A.; Baugh, K.; Jechow, A.; Hoelker, F.; Bennie, J.; Elvidge, C.D.; Gaston, K.J.; Guanter, L. Artificially lit surface of Earth at night increasing in radiance and extent. *Sci. Adv.* **2017**, *3*, e1701528. [CrossRef]
42. Falchi, F.; Cinzano, P.; Duriscoe, D.; Kyba, C.C.M.; Elvidge, C.D.; Baugh, K.; Portnov, B.A.; Rybnikova, N.A.; Furgoni, R. The new world atlas of artificial night sky brightness. *Sci. Adv.* **2016**, *2*, e1600377. [CrossRef]
43. Chinazzi, M.; Davis, J.T.; Ajelli, M.; Gioannini, C.; Litvinova, M.; Merler, S.; Pastore y Piontti, A.; Mu, K.; Rossi, L.; Sun, K.; et al. The effect of travel restrictions on the spread of the 2019 novel coronavirus (COVID-19) outbreak. *Science* **2020**, *368*, 395–400. [CrossRef] [PubMed]
44. Pal, S.; Das, P.; Mandal, I.; Sarda, R.; Mahato, S.; Nguyen, K.-A.; Liou, Y.-A.; Talukdar, S.; Debanshi, S.; Saha, T.K. Effects of lockdown due to COVID-19 outbreak on air quality and anthropogenic heat in an industrial belt of India. *J. Clean. Prod.* **2021**, *297*, 126674. [CrossRef] [PubMed]
45. Burns, J.; Movsisyan, A.; Stratil, J.M.; Coenen, M.; Emmert-Fees, K.M.F.; Geffert, K.; Hoffmann, S.; Horstick, O.; Laxy, M.; Pfadenhauer, L.M.; et al. Travel-related control measures to contain the COVID-19 pandemic: A rapid review. *Cochrane Database Syst. Rev.* **2020**, *10*, CD013717. [CrossRef] [PubMed]
46. Dingel, J.I.; Neiman, B. How many jobs can be done at home? *J. Public Econ.* **2020**, *189*, 104235. [CrossRef]
47. Wei, P.; Jin, C.; Xu, C. The Influence of the COVID-19 Pandemic on the Imports and Exports in China, Japan, and South Korea. *Front. Public Health* **2021**, *9*, 682693. [CrossRef]
48. Coronavirus Pandemic (COVID-19). Available online: https://ourworldindata.org/coronavirus (accessed on 1 February 2022).
49. Tu, T.H.L.; Hoang, T.M. The Impact of COVID-19 on Individual Industry Sectors: Evidence from Vietnam Stock Exchange. *J. Asian Financ. Econ. Bus.* **2021**, *8*, 91–101.
50. Seyedin, H.; Zanganeh, A.-M.; Mojtabaei, M.; Bagherzadeh, R.; Faghihi, H. A model of reopening businesses to decrease the heath and economic impacts of the COVID-19 pandemic: Lessons from Iran. *Med. J. Islam. Repub. Iran* **2020**, *34*, 97. [CrossRef]
51. Ministry of Commerce of the People's Republic of China. Available online: http://www.mofcom.gov.cn/article/i/jyjl/k/202103/20210303046598.shtml (accessed on 3 March 2021).
52. Ireland 2021: An Overview. Available online: https://partners.wsj.com/ida-ireland/advantage-ireland/ireland-2021-an-overview/?utm_source=wsj-search&utm_medium=CustomContentWSJ (accessed on 1 March 2021).
53. Awan, U.A.; Malik, M.W.; Khan, M.I.; Khattak, A.A.; Ahmed, H.; Hassan, U.; Qureshi, H.; Afzal, M.S. Predicting COVID-19 incidence in war-torn Afghanistan: A timely response is required! *J. Infect.* **2022**, *84*, E6–E8. [CrossRef]
54. Kouadio, H.K.; N'Guessan, R.K. Degree of sustainability of current account: Evidence from Cote d'Ivoire using a non-linear approach. *Heliyon* **2021**, *7*, e06589. [CrossRef]
55. Coulibaly, N.; Kone, S.; Casimir, G.K.; Berte, K.; Yapi, Y.M. Ripple effect, driving branch, and economic development: Case of the agro-food industry in Cote d'Ivoire. *Cienc. Rural* **2021**, *51*, e20200368. [CrossRef]
56. Ye, Y.; Deng, J.; Huang, L.; Zheng, Q.; Wang, K.; Tong, C.; Hong, Y. Modeling and Prediction of NPP-VIIRS Nighttime Light Imagery Based on Spatiotemporal Statistical Method. *IEEE Trans. Geosci. Remote Sens.* **2021**, *59*, 4934–4946. [CrossRef]
57. Cao, Z.; Wu, Z.; Kuang, Y.; Huang, N.; Wang, M. Coupling an Intercalibration of Radiance-Calibrated Nighttime Light Images and Land Use/Cover Data for Modeling and Analyzing the Distribution of GDP in Guangdong, China. *Sustainability* **2016**, *8*, 108. [CrossRef]
58. Hu, X.; Li, L.; Dong, K. What matters for regional economic resilience amid COVID-19? Evidence from cities in Northeast China. *Cities* **2022**, *120*, 103440. [CrossRef] [PubMed]
59. Ivan, K.; Holobaca, I.-H.; Benedek, J.; Torok, I. VIIRS Nighttime Light Data for Income Estimation at Local Level. *Remote Sens.* **2020**, *12*, 2950. [CrossRef]